High Performance Millimeter-Wave Image Reject Low-Noise Amplifier Using Inter-stage Tunable Resonators

Jihoon Kim and Youngwoo Kwon

A Q-band pHEMT image-rejection low-noise amplifier (IR-LNA) is presented using inter-stage tunable resonators. The inter-stage L-C resonators can maximize an image rejection by functioning as inter-stage matching circuits at an operating frequency (F_{OP}) and short circuits at an image frequency (F_{IM}). In addition, it also brings more wideband image rejection than conventional notch filters. Moreover, tunable varactors in L-C resonators not only compensate for the mismatch of an image frequency induced by the process variation or model error but can also change the image frequency according to a required RF frequency. The implemented pHEMT IR-LNA shows 54.3 dB maximum image rejection ratio (IRR). By changing the varactor bias, the image frequency shifts from 27 GHz to 37 GHz with over 40 dB IRR, a 19.1 dB to 17.6 dB peak gain, and 3.2 dB to 4.3 dB noise figure. To the best of the authors' knowledge, it shows the highest IRR and F_{IM}/F_{OP} of the reported millimeter/quasi-millimeter wave IR-LNAs.

Keywords: Q-band, image reject low-noise amplifier, IR-LNA, L-C resonators, varactor, image rejection ratio, IRR.

I. Introduction

The image problem is a typical problem of the superheterodyne system, which has been widely accepted in today's wireless applications. While the superheterodyne system has many advantages, such as respectable selectivity, sensitivity, and robustness, it inevitably requires image reject techniques [1], [2]. With each passing day, various millimeter-wave applications emerge in wireless areas; the image rejection in millimeter-wave systems becomes an increasingly more important aspect in providing a higher quality of service than ever before. Although the use of image reject filters in low-noise amplifiers (LNA) is a typical image rejection technique, it is difficult to implement very sharp band-pass filters for image rejection ratios over 20 dB in the millimeter-wave range. Therefore, Hartley and dual-intermediate frequency (IF) architecture, have been popularly adopted in receivers with millimeter-wave RF and low-IF frequencies (or, high F_{IM}/F_{OP}) [3]–[7]. However, they increase overall system complexity and DC power consumption—resulting from two-way mixers and extra-bulky IF couplers. Recently, image-reject-filtered LNAs are reported in not only microwave ranges but also in millimeter-wave or quasi-millimeter-wave ranges, as shown in Fig. 1 [3], [8]. Still, [3] needs the support of dual-IF architecture. Reference [8] is successfully implemented in the quasi-millimeter-wave frequency having over 50 dB IRR and high F_{IM}/F_{OP} (0.79), but it results in noise figure degradation by more than 1 dB due to use of the feedback notch circuit in the

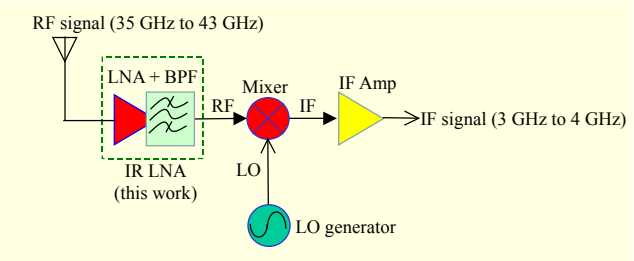

Fig. 1. Block diagram of superheterodyne receiver architecture.

Manuscript received July 9, 2013; revised Aug. 22, 2013; accepted Sept. 6, 2013.

This work was supported by the National Research Foundation of Korea (NRF) grant funded by the Korea Government (MEST, No. 0414-20120058), and the Acceleration Research Program of the Ministry of Education, Science and Technology of Republic of Korea, and the Korea Science and Engineering Foundation.

Jihoon Kim (phone: +82 2 880 8482, j7h7@snu.ac.kr) and Youngwoo Kwon (ykwon@snu.ac.kr) are with the Department of Electrical and Computer Engineering, Seoul National University, Seoul, Rep. of Korea.

first stage of LNA. Moreover, frequency shifting, induced from process variation and model error, imposes difficulty on sufficient image suppression at the required frequency. In this work, millimeter-wave image reject LNAs with high IRR-frequency tunable functions that have little noise figure degradation and high F_{IM}/F_{OP} are developed using inter-stage tunable resonators.

II. Inter-stage Tunable Resonators

Figure 2 shows a conventional notch filter and a series L-C resonator the input impedance of the latter changing less rapidly than the former according to the frequency. This is helpful in obtaining more wideband and higher image rejection characteristics. Although it can bring higher loss at the F_{OP} (here it is 35 GHz), this problem can be overcome by the fact that it can contribute to inter-stage matching as a common source structure at the F_{OP}. Figure 3 represents Y-parameter analysis for inter-stage matching. To simplify the analysis, we assume that the resonator consists of an ideal inductor and an ideal capacitor in series. A transistor can be modeled with intrinsic parameters while maintaining its size, as it was in the LNA. A gate-drain capacitance (C_{gd}) can be omitted, because it has only a minor effect on the inter-stage matching. Unless there are any other components at the inter-stage, usually the imaginary part of Y_L (imag(Y_L)) and Y_R (imag(Y_R)) are positive, as shown in (1), (2)

$$Y_L = g_{ds} + j\omega C_{ds}, \tag{1}$$

$$\begin{aligned} Y_R &= \frac{j\omega C}{1-\omega^2 LC} + \left(\omega^2 R_i C_{gs}{}^2 + j\omega C_{gs}\right) /\!/\; j\omega C_c \\ &\approx \frac{j\omega C}{1-\omega^2 LC} + j\omega C_{gs} \;/\!/\; j\omega C_c. \end{aligned} \tag{2}$$

However, by inserting an L-C resonator, the imag(Y_R) can reach a negative value by the first term added, because of the resonator's dependency upon frequency. It means that inter-stage matching is possible at a frequency whereby the imag(Y_L) is equal to –imag(Y_R). Thus, an LNA with a series L-C resonator can achieve almost the same gain as an LNA with a conventional notch filter at the F_{OP} retaining higher and more wideband rejection at the F_{IM} range. Figure 4 shows the schematic of the proposed image-reject low-noise amplifier. Inter-stage series resonators consist of inductors and varactors. Narrow and curved micro-strip lines are implemented as inductors. Varactors act as tunable capacitors in the resonators. Because they can change the resonating frequency depending on external biases, they can compensate for the mismatch of an image frequency induced from process variation and model error. In addition, it is possible to select an image frequency

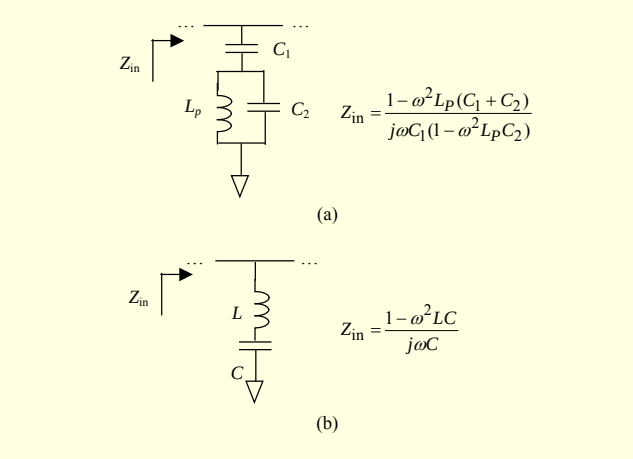

Fig. 2. Image rejection filters used in IR LNA: (a) conventional notch filter and (b) series resonator.

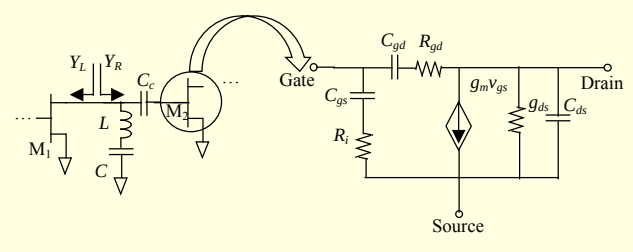

Fig. 3. Inter-stage matching analysis using simplified inter-stage resonator and small signal pHEMT equivalent circuit (intrinsic (Y_L (or Y_R): Y parameter looking toward an M_1 (or M_2) transistor)).

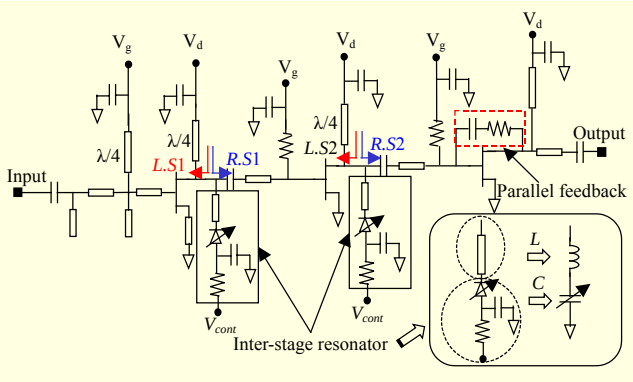

Fig. 4. Schematic of proposed IR LNA.

according to a required RF frequency. It means that with a single chip, practical use is possible for various applications inside the RF band. In this work, our target frequencies are 35 GHz and 43 GHz RF frequencies having 3 GHz to 4 GHz IF frequencies. As shown in Fig. 5, with the insertion of inter-stage resonators, LNAs result in not only short termination at an image frequency (27 GHz) but also inter-stage matching at an operating frequency (35 GHz) in both the first-second stage and second-third stage. This simulation result verifies our

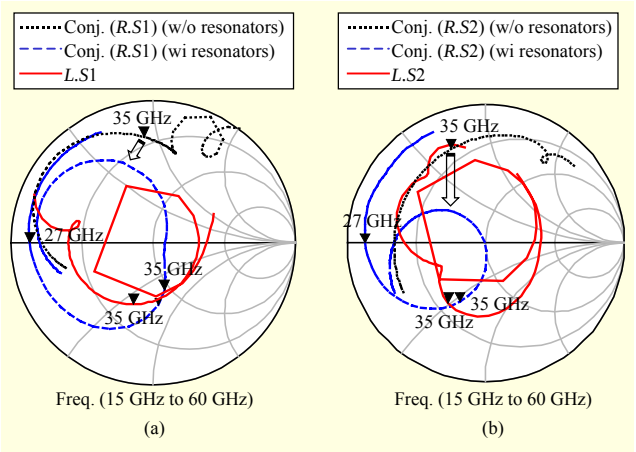

Fig. 5. Shifted trace of inter-stage matching circle before and after inserting inter-stage tunable resonators ((a): 1-2 stage and (b): 2-3 stage).

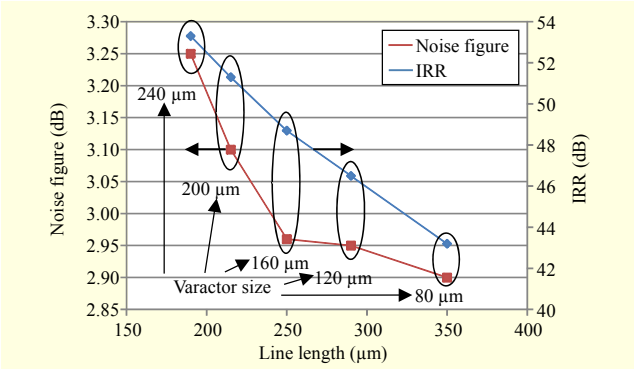

Fig. 6. Simulated IRR and noise figure of IR LNAs according to line length and varactor size (line width = 10 µm (fixed), resonating frequency = 27 GHz, and operating frequency = 35 GHz).

analysis, because it shows that the drastic change of the imaginary part of *R.S1* and *R.S2* at 35 GHz has a positive impact on inter-stage matching. The length of inductive lines and the size of varactors are the key parameters in designing the inter-stage tunable resonator. The optimum value is one that maximizes IRR and minimizes noise figure. Thus, the required trade-off between these specifications in determining line length and varactor size is as shown in Fig. 6. In this work, 250 µm line length and 4 × 40 µm (=160 µm) varactors are selected through careful simulation and analysis.

III. Measurements

The circuit has been fabricated using a commercial 0.15 µm GaAs pHEMT MMIC process with an f_T of 85 GHz and an f_{MAX} of 190 GHz. The chip size is 2.0 mm × 1.0 mm, as shown in Fig. 7. The measured scattering parameters (S-parameters) of the IR LNA show reasonable agreement with the simulated

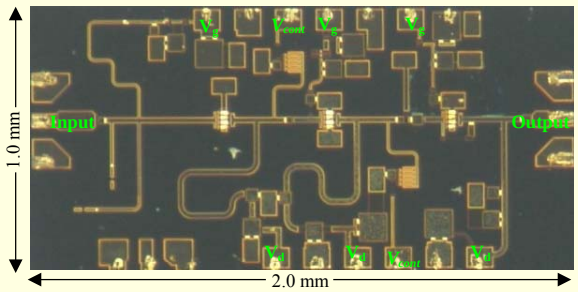

Fig. 7. Chip photo of proposed IR LNA.

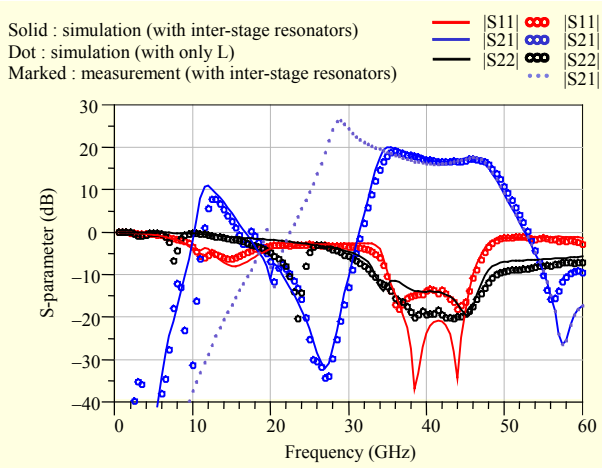

Fig. 8. Measured and simulated S-parameters of IR LNA (measurement: V_g = – 0.8 V, V_d = 1.5 V, V_{cont} = 2.1 V, and simulation: V_g = – 0.8 V, V_d =1.5 V, V_{cont} = 1.0 V).

results in Fig. 8. But the optimum varactor bias for the resonating image frequency (27 GHz) shifted from 1.0 V to 2.1 V. This result means that the bias-tuned varactor successfully compensates the mismatch induced from model error or process variation at high frequency.

The proposed IR LNA obtains 19.1 dB peak gain, 13 GHz gain bandwidth, and 52.2 dB IRR (when the image frequency is 27 GHz and the operating frequency is 35 GHz). If it is applied to a superheterodyne receiver, it can obtain 48 dB to 52 dB IRR within 1 GHz RF bandwidth, and over 20 dB IRR in 2 GHz to 9 GHz IF frequencies. The dotted line in Fig. 8 shows the simulated S21 when the inter-stages consist of only a single inductor (L) instead of L-C resonators. It means that L-C resonators play the role of matching circuits at the operating frequency and resonance circuits at the image frequency. Figure 9 represents the shifting of resonating frequency while sweeping the bias voltages of the varactor from 2.1 V to –1.8 V. As expected from the analysis, the proposed IR LNA makes it possible to adjust image frequency so that it can obtain the optimum IRR from 27 GHz to 37 GHz according to a wanted RF frequency. When V_{cont} = 2.1 V, it achieves 52.2 dB IRR (F_{OP} = 35 GHz and F_{IM} = 27 GHz) and 17.9 dB gain. When

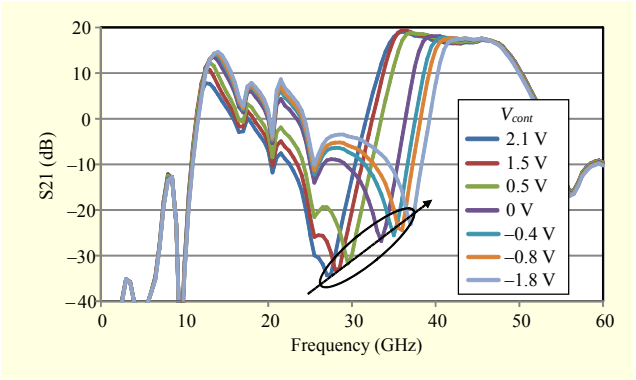

Fig. 9. Measured S21 of IR LNA vs. varactor bias.

Table 1. Comparison of millimeter wave/quasi-millimeter wave LNAs

Ref.	Tech.	F_{OP} (GHz)	F_{IM} (GHz)	Gain (dB)	NF (dB)	F_{IM}/F_{OP}	IRR (dB)
[3]	SiGe BiCMOS 0.13 µm	62	45	20	5.0	0.73	30
[8]	SiGe BiCMOS 0.18 µm	27.2	21.6	14	8.9	0.79	50.8
[9]	InAs/Alsb MHEMT	34 – 36	-	21.8	2.1	-	-
[10]	SOI CMOS 90 nm	26 – 42	-	11.9	3.6 – 4.2	-	-
[11]	InGaAs pHEMT 0.15 µm	29 – 43	-	14.2	2 – 3.3	-	-
This work	InGaAs pHEMT 0.15 µm	35.5	27.5	19.2	3.4	0.77	54.3
		43	37	17.4	4.3	0.86	40.5

V_{cont} = –1.8 V, it achieves 40.5 dB IRR (F_{OP} = 43 GHz and F_{IM} = 37 GHz) and 17.4 dB gain. Although it is not shown, input- and output-return loss also meet the requirement of below –10 dB at each operating frequency according to varactor bias. The variation of noise figure at the operating frequency is also measured when the varactor changes. If the resonating frequency shifts close to the operating frequency, gain starts to degrade in the operating frequency due to insertion loss from the inter-stage resonators. The loss plays the critical role to degrade noise figure. Table 1 summarizes the reported millimeter wave/quasi-millimeter wave IR LNAs or 30 GHz to 40 GHz LNAs. To the best of the authors' knowledge, it shows the highest IRR and F_{IM}/F_{OP} of the reported millimeter/quasi-millimeter wave IR LNAs with competent noise performance.

IV. Conclusion

A high performance pHEMT image reject LNA is demonstrated using inter-stage resonators. By positioning resonators in inter-stage, both inter-stage matching at an operating frequency and resonance at an image frequency, contribute to maximizing IRR. A tunable structure that uses varactors in the resonator successfully compensates the mismatched IRR at high frequency. Moreover, it makes it possible to utilize a single LNA in multi-standard superheterodyne applications that require high IRR. Finally, over 40 dB IRR is achieved having high F_{IM}/F_{OP} and moderate noise figure at both 35 GHz and 43 GHz from the proposed IR LNA.

References

[1] B. Razavi, *RF Microelectronics*, Englewood Cliffs, NJ: Prentice Hall, 1998.

[2] Y.-J. Ko, S.P. Stapleton, and R. Sobot, "Ku-Band Image Rejection Sliding-IF Transmitter in 0.13-µm CMOS Process," *IEEE Trans. Microw. Theory Tech.*, vol. 59, no. 8, Aug. 2011, pp. 2091–2107.

[3] S. Reynolds and B.A. Floyd, "A Silicon 60-GHz Receiver and Transmitter Chipset for Broadband Communications," *J. IEEE Solid-State Circuits*, vol. 41, no. 12, Dec. 2006, pp. 2820–2831.

[4] J. Kim et al., "60 GHz Broadband Image Rejection Receiver Using Varactor Tuning," *IEEE RFICs Symp.*, Anaheim, CA, USA, May 23–25, 2010, pp. 381–384.

[5] S.E. Gunnarsson et al., "60 GHz Single-Chip Front-End MMICs and Systems for Multi-Gb/s Wireless Communication," *J. IEEE Solid-State Circuits*, vol. 42, no. 5, May 2007, pp. 1143–1157.

[6] B. Razavi, "A Millimeter-Wave CMOS Heterodyne Receiver with on-Chip LO and Divider," *J. IEEE Solid-State Circuits*, vol. 43, no. 2, Feb. 2008, pp. 477–485.

[7] Y-H Chen, H.-H. Hsieh, and L.-H. Lu, "A 24-GHz Receiver Frontend with LO Signal Generator in 0.18-µm CMOS," *IEEE Trans. Microw. Theory Tech.*, vol. 56, no. 5, May 2008, pp. 1043–1051.

[8] T. Masuda et al., "A 50-dB Image-Rejection SiGe-HBT-Based Low Noise Amplifier in 24-GHz Band," *IEEE RFICs Symp.*, Boston, MA, USA, June 7–9, 2009, pp. 307–310.

[9] J.B. Hacker et al., "An Ultra-low Power InAs/AlSb HEMT Ka-Band Low-Noise Amplifier," *IEEE Microw. Wireless Compon. Lett.*, vol. 14, no. 4, Apr. 2004, pp. 156–158.

[10] F. Ellinger, "26–42 GHz SOI CMOS Low-Noise Amplifier," *J. IEEE Solid-State Circuits*, vol. 39, no. 3, Mar. 2004, pp. 522–528.

[11] Y. Yu, W. Hsu, and Y.E. Chen, "A Ka-Band Low Noise Amplifier Using Forward Combining Technique," *IEEE Microw. Wireless Compon. Lett.*, vol. 20, no. 12, Dec. 2010, pp. 672–674.